Article

Extending NMR Quantum Computation Systems by Employing Compounds with Several Heavy Metals as Qubits

Jéssica Boreli dos Reis Lino [1], Mateus Aquino Gonçalves [1], Stephan P. A. Sauer [2,*]
and Teodorico Castro Ramalho [1,3]

[1] Department of Chemistry, Federal University of Lavras, Lavras 37200-000, Brazil; jessicaboreli@outlook.com (J.B.d.R.L.); mateus.a.g@hotmail.com (M.A.G.); teodorico.ramalho@gmail.com (T.C.R.)
[2] Department of Chemistry, University of Copenhagen, DK-2100 Copenhagen, Denmark
[3] Center for Basic and Applied Research, Faculty of Informatics and Management, University Hradec Kralove, 50003 Hradec Kralove, Czech Republic
[*] Correspondence: sauer@chem.ku.dk

Abstract: Nuclear magnetic resonance (NMR) is a spectroscopic method that can be applied to several areas. Currently, this technique is also being used as an experimental quantum simulator, where nuclear spins are employed as quantum bits or qubits. The present work is devoted to studying heavy metal complexes as possible candidates to act as qubit molecules. Nuclei such ^{113}Cd, ^{199}Hg, ^{125}Te, and ^{77}Se assembled with the most common employed nuclei in NMR-QIP implementations (^{1}H, ^{13}C, ^{19}F, ^{29}Si, and ^{31}P) could potentially be used in heteronuclear systems for NMR-QIP implementations. Hence, aiming to contribute to the development of future scalable heteronuclear spin systems, we specially designed four complexes, based on the auspicious qubit systems proposed in our previous work, which will be explored by quantum chemical calculations of their NMR parameters and proposed as suitable qubit molecules. Chemical shifts and spin–spin coupling constants in four complexes were examined using the spin–orbit zeroth-order regular approximation (ZORA) at the density functional theory (DFT) level, as well as the relaxation parameters (T_1 and T_2). Examining the required spectral properties of NMR-QIP, all the designed complexes were found to be promising candidates for qubit molecules.

Keywords: NMR; NMR parameter calculations; qubit molecules; quantum information processing; quantum dynamics

1. Introduction

Nuclear resonance magnetic (NMR) is a celebrated technique with plenty of applications in chemistry, physics, medicine, and structural biology. Besides its well-known uses, such as identifying molecules and determining their structure and dynamics, NMR has also been used as a experimental quantum simulator [1], where nuclear spins are employed as quantum bits or qubits—the fundamental information unit used in quantum information processing (QIP) [2].

Meanwhile, the advancement of the aimed at large-scale NMR quantum processors depends mainly on two challenges: first, the accurate and efficient control of the quantum system states; second, the construction of systems containing a large number of qubits [3]. The former have been augmented by the development of algorithms that are able to manipulate, with high fidelity, the quantum states of relatively large systems [4]. Recently, Peterson et al. [5] designed a fast and scalable algorithm for controlling the quantum states of systems containing 100 qubits.

These recent algorithms combined with modern NMR equipment and sophisticated theoretical techniques make possible the manipulation of the nuclear spin system states

through magnetic radiofrequency (RF) pulses, which are used to implement quantum gates, the basic computational step [5].

Regarding the second challenge, chemistry can leverage the development of NMR large-scale quantum systems, as it depends especially on the design of a qubit molecule containing a large number of suitable spin-1/2 nuclei, which act as the qubits. The properties that determine whether a molecule is suitable as a QIP molecule are—apart from of course the stability of the molecule—its NMR parameters such as the chemical shifts and the indirect nuclear spin–spin coupling constants [6]. These two molecular properties can currently accurately and efficiently be calculated by various quantum chemical methods [7–12]. The most widely employed of them is certainly density functional theory (DFT). The natural sequence of designing molecules is today therefore to screen potential candidate molecules by quantum chemical calculations of their relevant properties prior to an actual synthesis. In this way, theoretical chemistry can speed up the sharpening of the potential QIP molecule concerning its physical requirements [13], towards a specially synthesized system, giving resolvable spectra to the upcoming large-scale NMR quantum processor.

Nuclear spins-1/2 are natural qubits and are therefore widely used in NMR-QIP, where systems containing ^{1}H, ^{13}C, ^{19}F, ^{29}Si, and ^{31}P nuclei are the most employed ones [3,14,15]. Furthermore, other spin-1/2 nuclei, such as ^{113}Cd, ^{199}Hg, ^{125}Te, and ^{77}Se nuclei, have been investigated as qubits, and assembled with the most commonly employed nuclei, they could potentially be used in heteronuclear systems for NMR-QIP implementations.

NMR-QIP is usually implemented in an ensemble of identical and non-interacting molecules at room temperature [3]. An NMR quantum computer with n qubits requires a molecule with n coupled spin-1/2 [16]. This qubit molecule should present appropriate NMR parameters for QIP's efficient implementation, these being [14,16,17]: (i) large spin–spin coupling constants (J) between directly coupled spins, as the typical time required for two-qubit quantum gates is inversely proportional to the size of the coupling between the two coupled nuclei; (ii) a large range of chemical shifts; the frequency differences of the nuclei should be as large as possible to allow the selective manipulation of the individual spins, which is a basic computational step; (iii) the relaxation time of the nuclei should also be large enough to perform a huge number of logic quantum gates in a given algorithm.

In our previous studies, we investigated suitable qubit molecules, as well as suggested structural modifications of them, with the aim to enhance their NMR parameters for the QIP efficient implementation. Lino et al. [16] theoretically explored benzyldene-2,3-dihydro-1H-[1,3]diphosphole (BDF) derivatives in order to develop new promising phosphorus heterocycle compounds for QIP. The BDF–NO$_2$ derivative was found to be the best candidate for NMR quantum computations among the studied phosphorus heterocycles containing π-conjugated molecular skeletons.

In our following work [18], exceptionally large through-space (TS) P-P spin–spin coupling constants observed in 1,8-diphosphanaphthalenes (PPN) and in naphtho[1,8-cd]-1,2-dithiole phenylphosphines (NTP) were proposed and investigated to provide more accurate control within large-scale NMR-QIP. We explored the large TS J ^{31}P-^{31}P couplings to provide tighter, more accurate control through large-scale NMR-QIP, proposing the application of TS J(^{31}P,^{31}P) coupling as a resource for universal logic in NMR quantum computers. From our results, PPN$_o$–F, PPN$_o$–ethyl, and PPN$_o$–NH$_2$ were the best candidates for NMR-QIP, in which the large TS SSCCs could face the need for long-time quantum gates' implementations. The following work [19] was devoted to evaluating and calculating directly the relaxation parameters of the suitable qubit molecules proposed in the last mentioned work. In NMR-QIP, decoherence is a key problem, and considering the unique qubits, the time of the coherence phase can be well measured by the time of transversal relaxation (T_2), wherein the longer the relaxation time, the better the information processing is. The relaxation parameters (T_1 and T_2) of the molecules PPN$_o$–F, PPN$_o$–ethyl, and PPN$_o$–NH$_2$ were calculated, and the results supported and confirmed that they are suitable

qubit molecules, which could improve the control accuracy through large-scale NMR-QIP, highlighted by the promising longer coherence time, avoiding a high decoherence rate.

Along the same lines, our latest work [20] focused on heteronuclear systems with heavy metals such as ^{113}Cd, ^{199}Hg, ^{77}Se, and ^{125}Te as qubits for NMR-QIP. We examined the NMR parameters of metal complexes with phosphine chalcogenide ligands (called MRE) using spin–orbit ZORA and four-component relativistic methods. We developed a computational design strategy for prescreening molecules that could enable many and heteronuclear qubits for NMR-QIP implementations. Particularly, the influence of different conformers, basis sets, functionals, and methods to treat the relativistic, as well as solvent effects was studied. The MRE complexes were found to be multiple-spin systems with Larmor frequencies appropriately dispersed, so well-defined qubits, allowing qubit addressability, together with an exceptionally large spin–spin coupling between the pair of spins, which enables the two-qubit operations.

In this work, we aimed to go a step further in relation to the use of heavy metals (^{113}Cd, ^{199}Hg, ^{77}Se, and ^{125}Te) as qubits. Supported by the findings of our last mentioned work [20], the use of heavy metals combined with the most frequently used qubits (^{1}H, ^{13}C, ^{19}F, ^{29}Si, and ^{31}P) can boost the emergent scalable heteronuclear spin system in NMR-QIP. An NMR computer can be programmed electronically analogously to a quantum computer, but also, it can be implemented at room pressure and temperature using macroscopic liquid samples [21]. Thereby, we specially designed four complexes, still based on the auspicious qubit systems proposed in our work [20], which will be explored by quantum chemical calculations of their NMR parameters in order to investigate their suitability as qubit molecules.

2. Computational Details

Geometry optimizations and vibrational frequency calculations of all compounds were performed with the ORCA 4.2 program [22] at the DFT level in the framework of the two-component relativistic zeroth-order regular approximation (ZORA) [23] with the PBE0 exchange-correlation functional and ZORA–def2–TZVP basis set [24]. The SARC–ZORA–TZVP [24] basis set was used for Hg and the old–ZORA–TZVP was used for Cd, Te, and Se. The segmented all-electron relativistically contracted (SARC/J) basis sets were used in all ORCA calculations as the auxiliary basis sets. The SARC/J auxiliary basis set is a decontracted def2/J auxiliary. Corresponding frequency calculations confirmed that the geometries were indeed minima. The Cartesian coordinates of all optimized structures of the isolated molecule and vibrational frequencies are given in the Supplementary Material.

The NMR parameters of the studied complexes were investigated for the isolated molecule at the DFT level also in the ZORA framework, including spin–orbit effects and the Gaussian finite nucleus, as implemented in the Amsterdam density functional (ADF) program [25]. The calculations of the absolute nuclear magnetic shielding constants σ were carried out with the PBE0 exchange-correlation functional together with the triple-ζ (TZ2P) Slater-type basis set [26]. Gauge including atomic orbitals were employed in these calculations. The indirect spin–spin coupling constants (SSCC or J) were evaluated also with the PBE0 functional, but with the TZ2P–J Slater-type basis set [27], which is specially designed for NMR SSCC calculations. Those two theoretical levels were studied in our previous work and exhibited the best performance within the performed benchmarking [20,28–31]. One should note, however, that in a recent study, it was shown that Dyall's energy-optimized Gaussian-type basis sets had to be extended with additional f-type functions in order to obtain convergence for spin–spin coupling constants in correlated wave function calculations at the SOPPA(CCSD) level [32]. Whether this also would be the case for the Slater-type basis sets and DFT calculations needs to be seen.

For the present work, the two-component spin–orbit ZORA method was used. This approach has been successfully applied in several systems involving transition metals, including all atoms of the systems used in this work [29,31,33–35]. From a previous study,

the concomitant changes in the NMR spectroscopy parameters were, in general, small going from the ZORA calculation to the four-component DKS approach [20].

NMR chemical shifts (δ) were calculated relative to: tetramethylsilane ($Si(CH_3)_4$, TMS) for ^1H, ^{13}C, and ^{29}Si; $CFCl_3$ for ^{19}F; PH_3 for ^{31}P; $SeMe_2$ for ^{77}Se; $TeMe_2$ for ^{125}Te; $CdMe_2$ for ^{113}Cd; $HgMe_2$ for ^{199}Hg. All these references compounds were optimized and calculated at the same level as mentioned before. Table 1 shows the individual absolute shieldings. The chemical shifts (δ in ppm) of the nucleus (N) were then calculated as:

$$\delta_N = \frac{\sigma_{reference} - \sigma_N}{1 - \sigma_{reference}} \times 10^6. \tag{1}$$

The ^{31}P and ^{113}Cd chemical shifts were subsequently corrected by the gas phase experimental value of $CdMe_2$, -706.15 ppm [36], and PH_3, -266.1 ppm [37], as they are not the reference compounds of the standard chemical shift scale for Cd and P. Comparing our calculated absolute shielding constant for the carbon in TMS, 191.3 ppm, with a value of 188.1 ppm from a semi-experimentally derived absolute shielding scale [38] showed good agreement, taking into account that our value is for the equilibrium geometry, while the experimentally derived value is still for 300 K. In addition, one should recall that calculated chemical shifts or differences in Larmor frequencies, as we study here, are normally more accurate due to error cancellations.

Table 1. ^1H, ^{13}C, ^{29}Si, ^{19}F, ^{31}P, ^{77}Se, ^{125}Te, ^{113}Cd, and ^{199}Hg NMR absolute shieldings, σ (ppm) of the (($Si(CH_3)_4$, TMS), $CFCl_3$, PH_3, $SeMe_2$, $TeMe_2$, $CdMe_2$, and $HgMe_2$ reference molecules. Calculated using the two-component ZORA approach with the PBE0 exchange-correlation functional and the TZ2P basis sets.

Nucleus	Shielding	Nucleus	Shielding
σ Hg ($HgMe_2$)	9197.834	σ Si (TMS)	368.108
σ Cd ($CdMe_2$)	3561.291	σ F ($CFCl_3$)	184.172
σ Te ($TeMe_2$)	3557.070	σ C (TMS)	191.333
σ Se ($SeMe_2$)	1930.599	σ H (TMS)	31.553
σ P (PH_3)	607.566		

Whilst the herein employed theoretical model provides insightful information on the relationship between structure and spectroscopic properties, the clear practical utility lies in its ability to predict the performance of unique molecule classes, thereby directing future efforts. In this line, quantum chemical calculations performed on isolated molecules are useful, as a first approach, to rationalize qubit molecules. Later on, more sophisticated calculations can be employed to introduce thermal and solvent or environment effects, thus making the model more realistic.

Molecular dynamics (MD) simulations were carried out in the ORCA 4.2 program [22], using the functional PBE with the basis set ZORA-def2-TZVP; the temperature of 300 K was included in all MD simulations. The simulation consisted of a thermalization stage of 1 ps, obtaining a total of 1000 conformations. After the MD simulations, we obtained the relaxation times (T_1 and T_2) and relaxation rates (r_1 and r_2) of the atoms by means of the spectral density. This methodology has already been used successfully in other works [19,39,40]; it uses the distance between two atoms for each conformation selected by the procedure of statistical inefficiency. That way, the parameters T_1 and T_2 were obtained by the spectral density method in the MATLAB 7.6 software [41]. For more datails, please see [19,39].

3. Results and Discussion

The complexes proposed and investigated in this work are $HgF_2[((CH_3)_3SiCH_2)(CH_3)Te][(C_4H_8N)(CH_3)HPTe]$, $HgF_2[((CH_3)_3SiCH_2)(CH_3)Se][(C_4H_8N)(CH_3)HPSe]$,

$CdF_2[((CH_3)_3SiCH_2)(CH_3)Te][(C_4H_8N)(CH_3)HPTe]$, and
$CdF_2[((CH_3)_3SiCH_2)(CH_3)Se][(C_4H_8N)(CH_3)HPSe]$,
which are denoted as complex 1, complex 2, complex 3, and complex 4 throughout the article (Figure 1). These complexes were theoretically designed based on the complexes and heavy atoms studied in our previous work [20] and pointed out as auspicious qubit molecules. In this work, structure modifications were performed in a way that all the basic requirements for NMR-QIP were fulfilled. These modifications were based on fragments of chemical structures previously synthesized [42–44]. Although the proposed molecules studied in this work have not been synthesized yet, they are based on structures already constructed and could, in principal, be synthesized as well.

3.1. Conformational Flexibility

In our previous work [20], we investigated the influence of different conformers in the calculations of the NMR parameters. We carried out a conformer search using Open Babel 2.4.1 [45], and up to 50 conformers were generated in order to identify other conformations. From the Boltzmann averaging, we observed only small variations in both δ and J and concluded, for this reason, that there is no need to perform calculations of the NMR parameters for all the main conformers. Therefore, we followed the trends here in this work and kept working with only one optimized geometry. Therefore, starting from an optimized geometry of each complex, the NMR parameters were calculated at the ZORA/PBE0/TZ2P level for chemical shifts and ZORA/PBE0/TZ2P-J for spin–spin couplings.
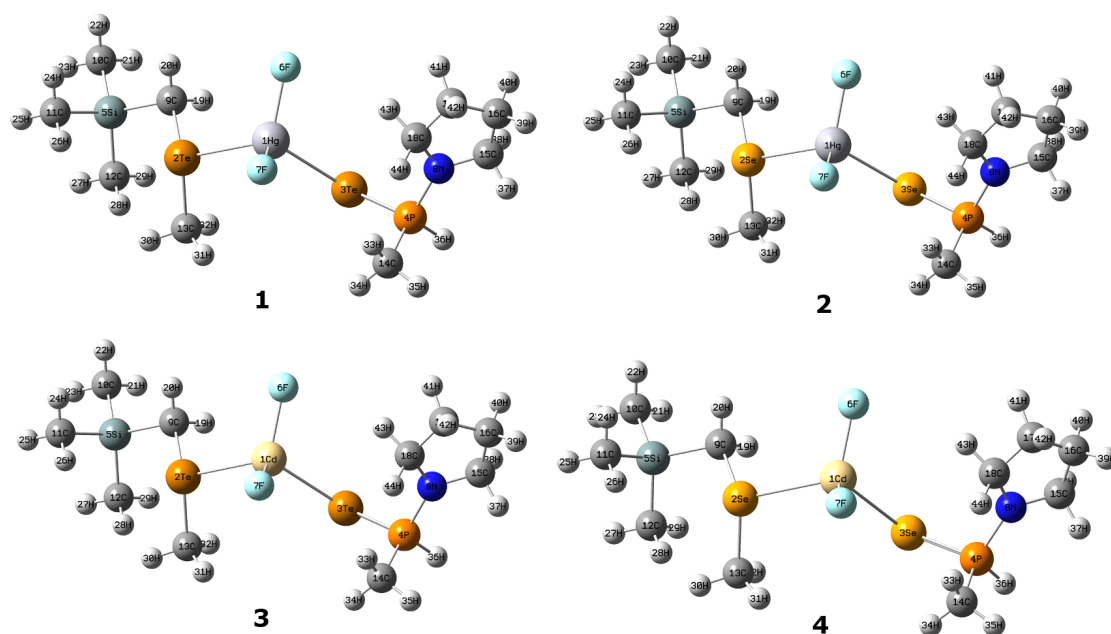

Figure 1. Studied complexes HgF2[((CH3)3SiCH2)(CH3)Te][(C4H8N)(CH3)HPTe] (complex 1), HgF2[((CH3)3SiCH2)(CH3)Se][(C4H8N)(CH3)HPSe] (complex 2), CdF2[((CH3)3SiCH2) (CH3)Te][(C4H8N)(CH3)HPTe] (complex 3), and CdF2[((CH3)3SiCH2)(CH3)Se][(C4H8N)(CH3)HPSe] (complex 4).

3.2. Spectroscopic Parameters: Chemical Shift Values

The designed structure of the complexes proposed in this work could overcome the restriction regarding the number of suitable qubits for the forthcoming NMR quantum computer. The chemical shifts of the studied molecules are shown in Table 2. As expected, the complexes presented a huge range of chemical shifts, when all the nuclei were taken into account, as we dealt with heterogeneous systems. Complex 1 exhibited the biggest chemical shift range, 1567 ppm, varying from −1513.02 ppm for Hg1 to 53.53 ppm for C15. Complex 2 presented the second biggest range, which was 1447 ppm, varying from

−1387.93 for Hg1 to 58.59 for Se3. The following range is given by complex 3: the range of chemical shifts was 1027 ppm, varying from −700.37 for Te3 to 326.71 for Hg1. The smallest range was seen in complex 4, which was 554 ppm, varying from −250.82 for Te3 to 303.00 for Hg1. In summary, Hg complexes showed the widest chemical shift range; these results are as expected, as Hg spans a wider chemical shift range compared to Cd.

The different chemical shifts afforded to each nucleus in the complexes are a reflection of the different electronic environments in the molecules. When nuclei have distinct gyromagnetic ratios γ; they provide qubits that can easily be individually addressed through RF pulses [46]. Hence, using different spin-1/2 nuclei in differing chemical environments is a kick off for scaling up NMR quantum computers.

Table 2. Chemical shifts ($M = {}^{113}$Cd or ^{199}Hg and $E = {}^{77}$Se or ^{125}Te), δ (ppm) calculated using the two-component ZORA approach with the PBE0 exchange-correlation functional and the TZ2P basis sets.

Nucleus	Complex 1	Complex 2	Complex 3	Complex 4
δM	−1513.02	−1387.93	326.71	303.00
$\delta E2$	−46.23	58.59	−188.55	−10.28
$\delta E3$	−565.29	−195.80	−700.37	−250.82
$\delta P4$	−18.67	25.03	−22.51	24.25
$\delta Si5$	4.41	3.00	4.50	2.32
$\delta F6$	−202.22	−220.33	−231.50	−244.14
$\delta F7$	−148.50	−145.68	−175.97	−185.88
$\delta C9$	1.59	20.69	−2.00	19.18
$\delta C10$	−1.01	−0.34	−0.92	1.26
$\delta C11$	0.06	−1.01	−0.23	−1.77
$\delta C12$	−0.65	−1.88	−0.74	−1.03
$\delta C13$	−6.62	15.57	−8.88	14.59
$\delta C14$	20.48	19.14	19.63	18.47
$\delta C15$	53.53	50.95	53.88	50.77
$\delta C16$	28.63	29.00	28.71	29.31
$\delta C17$	30.96	30.70	30.23	30.09
$\delta C18$	51.55	51.47	50.72	50.66
$\delta C19$	1.38	1.47	1.39	1.73
$\delta C20$	4.22	3.71	3.43	3.66
$\delta C21$	−0.03	0.27	0.35	−0.03
$\delta C22$	0.95	−0.05	−0.03	0.16
$\delta C23$	−0.13	−0.02	−0.03	0.04
$\delta C24$	1.71	−0.08	0.02	0.02
$\delta C25$	−0.14	−0.14	−0.03	−0.22
$\delta C26$	−0.19	1.16	0.51	2.50
$\delta C27$	−0.03	−0.15	−0.14	0.07
$\delta C28$	0.26	1.56	1.98	0.24
$\delta C29$	−0.02	−0.01	−0.22	0.02
$\delta C30$	1.38	1.59	1.47	1.85
$\delta C31$	1.44	1.72	1.42	1.84
$\delta C32$	6.07	5.64	5.27	3.82
$\delta C33$	7.62	7.09	6.34	5.75
$\delta C34$	1.66	1.54	1.67	1.53
$\delta C35$	2.63	2.01	2.66	2.04
$\delta C36$	7.76	8.30	7.57	8.15
$\delta C37$	2.45	2.62	2.43	2.57
$\delta C38$	3.36	3.62	3.54	3.85
$\delta C39$	1.45	1.46	1.40	1.47
$\delta C40$	3.76	3.98	4.03	3.90

Table 2. *Cont.*

Nucleus	Complex 1	Complex 2	Complex 3	Complex 4
$\delta C41$	2.11	2.09	2.14	2.07
$\delta C42$	1.62	1.65	1.66	1.70
$\delta C43$	4.50	4.60	4.55	4.82
$\delta C44$	2.74	2.85	2.76	2.85

3.3. Spectroscopic Parameters: Spin–Spin Coupling Constant Values

For multiple-spin systems, while homonuclear spins are often individually addressed by the distinct δ due to different local environments, heteronuclear spins are easily distinguished due to the distinct nuclear gyromagnetic ratio γ and, thus, very different Larmor frequencies ω_0 [4]. Taking this into account, further in the paper, we discuss the NMR-QIP prerequisite of the large chemical shift range in terms of the frequency differences of the coupled nuclei. The nuclei Larmor frequencies of the studied complexes are shown in Tables S3–S6.

To evaluate the relative magnitudes of the spin–spin coupling constant in consonance with the spread in the Larmor frequencies, one needs to come back to the foundations of NMR quantum computing [17]. Quantum logic gates were implemented through RF pulses based on a scalar coupling Hamiltonian [47]. The Hamiltonian for scalar J-coupling of a molecule containing N spin-1/2 coupled nuclei is given by:

$$H_J = \frac{\hbar\pi}{2} \sum_{K<L}^{N} J_{KL} I^K I^L = \frac{\hbar\pi}{2} \sum_{K<L}^{N} J_{KL}(I_x^K I_x^L + I_y^K I_y^L + I_z^K I_z^L), \tag{2}$$

where J_{KL} is the coupling strength between the spins K and L. In Equation (2), the system is said to be strongly coupled. When the frequency separation between the spins $\omega_0^K - \omega_0^L$ is large compared to their coupling strength, i.e., when $|J_{KL}| \ll |\omega_0^K - \omega_0^L|$, one can simplify Equation (2) to

$$H_J = \frac{\hbar\pi}{2} \sum_{K<L}^{N} J_{KL} I_z^K I_z^L. \tag{3}$$

When the condition $|J_{KL}| \ll |\omega_0^K - \omega_0^L|$ applies, the spectra are also said to be first order and the system is said to be weakly coupled; this is also known as the minimal coupling approximation. This condition is easily satisfied for heteronuclear spins and for small homonuclear molecules when the chemical shift between the nuclei is sufficiently large. Mawhinney and Schreckenbach [17] demonstrated that the differences in chemical shifts and the spin–spin coupling between nuclei are not required to be extremely large. Therefore, they evaluated the required spectral properties and concluded that what is actually required for a first-order spectrum is a relationship of $\frac{\Delta\omega_0}{J} \geq 10$ [48].

Hence, in compliance with minimal coupling approximation and in line with the criteria proposed by Mawhinney and Schreckenbach [17], we examined the required spectral properties for NMR-QIP, evaluating the ratio $\frac{\Delta\omega_0}{J} \geq 10$ for all the designed complexes. The ratio analysis of the studied complexes is shown in Tables S7–S10. We first investigated the directed coupled nuclei, because even though the nuclei do not need to be mutually coupled, they must form a contiguous network of couplings [17]. The spin–spin coupling constant for directed coupled nuclei and the difference in the Larmor frequencies (for a 16.5 T magnet) between coupled nuclei are displayed in Table 3. Taking into account all four complexes, all the pairs of nuclei exhibited a ratio grater than 10. The smallest ratio was 5658 for the pair of nuclei Hg1–Se3 in complex 2, and the largest ratio was 5,172,004 for the pair P4–C14 in complex 1.

Table 3. Spin–spin coupling constants for directed coupled nuclei (M = ^{113}Cd or ^{199}Hg and E = ^{77}Se or ^{125}Te), J (Hz), and differences in the Larmor frequencies (for a 16.5 T magnet) between the coupled nuclei, $\Delta\omega_0$ (Hz).

	Complex 1		Complex 2		Complex 3		Complex 4	
	^1J	$\Delta\omega_0$	^1J	$\Delta\omega_0$	^1J	$\Delta\omega_0$	^1J	$\Delta\omega_0$
M1–E2	3302.70	96,802,165	−835.01	8,435,780	−481.12	66,742,136	105.44	21,582,334
M1–E3	5102.88	96,686,569	−1485.00	8,401,607	−878.27	66,628,154	233.79	21,614,648
M1–F6	−2621.28	535,132,459	−2483.84	535,104,716	783.72	505,084,765	677.95	505,080,108
M1–F7	−2405.23	535,167,977	−2330.77	535,154,067	784.66	505,121,481	691.68	505,118,628
E2–C9	−15.82	46,039,162	−83.82	42,314,827	195.52	46,008,099	−81.18	42,323,811
E2–C13	−24.25	46,040,612	−69.38	42,313,921	163.74	46,009,316	−69.04	42,322,999
E3–P4	1411.66	61,967,771	−607.71	150,249,393	1504.62	61,996,763	−660.24	150,256,563
P4–C14	20.86	107,887,999	28.34	107,900,668	22.47	107,887,060	29.75	107,900,565
P4–H36	422.22	417,965,157	448.08	417,953,108	428.45	417,966,118	451.89	417,953,223
Si5–C9	−34.38	37,025,106	−34.41	37,028,676	−33.74	37,024,459	−32.89	37,028,505
Si5–C10	−41.49	37,024,645	−37.33	37,024,961	−38.53	37,024,649	−39.00	37,025,340
Si5–C11	−41.75	37,024,835	−42.01	37,024,843	−40.35	37,024,771	−42.09	37,024,804
Si5–C12	−37.53	37,024,710	−41.88	37,024,688	−41.38	37,024,681	−39.32	37,024,935
C15–C16	26.44	4398	26.40	3878	26.27	4447	26.22	3791
C16–C17	23.53	410	23.53	300	23.64	268	23.76	138
C17–C18	26.76	3637	26.82	3670	26.85	3620	26.73	3634
C9–H19	123.68	525,852,016	122.91	525,848,702	123.92	525,852,654	124.00	525,849,153
C9–H20	135.65	525,854,011	136.23	525,850,273	133.03	525,854,085	132.86	525,850,508
C10–H21	112.77	525,851,482	111.88	525,851,574	112.46	525,851,732	112.68	525,851,083
C10–H22	117.10	525,852,170	112.07	525,851,354	112.23	525,851,464	112.86	525,851,213
C10–H23	112.22	525,851,414	111.99	525,851,373	111.84	525,851,467	112.27	525,851,130
C11–H24	119.40	525,852,519	112.53	525,851,447	112.84	525,851,377	112.07	525,851,650
C11–H25	111.88	525,851,220	112.21	525,851,409	112.37	525,851,343	110.23	525,851,481
C11–H26	110.67	525,851,181	118.19	525,852,321	115.41	525,851,725	120.02	525,853,393
C12–H27	112.02	525,851,417	111.54	525,851,552	111.82	525,851,358	112.22	525,851,556
C12–H28	111.68	525,851,624	119.15	525,852,752	119.44	525,852,844	113.36	525,851,678
C12–H29	112.20	525,851,429	111.67	525,851,649	110.88	525,851,304	113.30	525,851,523
C13–H30	132.24	525,853,467	131.56	525,849,693	132.76	525,853,929	133.17	525,850,045
C13–H31	129.49	525,853,505	127.68	525,849,787	128.90	525,853,895	128.17	525,850,038
C13–H32	151.11	525,856,759	150.06	525,852,540	150.00	525,856,598	144.53	525,851,434
C14–H33	134.29	525,853,058	133.34	525,852,924	133.78	525,852,312	133.42	525,852,103
C14–H34	123.44	525,848,870	123.40	525,849,024	123.77	525,849,030	123.26	525,849,137
C14–H35	121.84	52,5849,553	121.41	525,849,354	121.87	525,849,729	120.86	525,849,499
C15–H37	129.93	525,843,591	129.48	525,844,164	130.37	525,843,517	129.55	525,844,160
C15–H38	128.27	525,844,233	129.07	525,844,865	128.31	525,844,291	129.42	525,845,060
C16–H39	121.40	525,847,283	121.31	525,847,231	121.09	525,847,240	121.22	525,847,184
C16–H40	129.67	525,848,911	130.16	525,848,998	130.18	525,849,087	129.51	525,848,891
C17–H41	126.03	525,847,341	125.78	525,847,371	125.49	525,847,492	124.91	525,847,466
C17–H42	116.70	525,846,995	116.72	525,847,064	116.85	525,847,149	117.18	525,847,205
C18–H43	141.85	525,845,384	141.07	525,845,467	138.72	525,845,563	137.77	525,845,763
C18–H44	129.44	525,844,147	129.09	525,844,233	129.06	525,844,302	129.05	525,844,379

Analyzing the individual complexes and starting with the Hg complexes, for complex 1 with Te, the smallest ratio, 17, was observed for the pair of nuclei C16–C17, which exhibited a J-coupling constant of 23.53 Hz and a Larmor frequency difference of 410 Hz. At the other end of the range, the largest ratio, 5,172,004, was found for the pair of nuclei P4–C14, which had a J-coupling constant of 20.86 Hz and a Larmor frequency difference of 107,887,999 Hz. For complex 2 with Hg and Se, the smallest ratio, 13, was predicted for the pair of nuclei C16–C17, which exhibited a J-coupling constant of 23.53 Hz and the smallest Larmor frequency difference of 300 Hz. The largest ratio, 4,714,635, was found for the pair of nuclei C12–H27 for which the J-coupling constant was 111.54 Hz and the Larmor frequency difference was 525,851,552 Hz. Concerning the Cd complexes, complex 3 with Te exhibited also for the pair of nuclei C16–C17 the smallest ratio, 11, with a J-coupling

constant of 23.64 Hz and a Larmor frequency difference of 268 Hz. The biggest ratio, 4,801,382, was shown by P4–C14, with a J-coupling constant of 22.47 Hz and a Larmor frequency difference of 107,887,060 Hz. The last complex, complex 4 with Cd and Se, exhibited the smallest ratio of 6 for the pair of nuclei C16–C17, for which the J-coupling constant was 23.76 Hz and the Larmor frequency difference was 138 Hz. The largest ratio was presented by C11–H25, with a J-coupling constant of 110.23 Hz and a Larmor frequency of 525,851,481 Hz. As mentioned above, the pair of nuclei C16–C17 presented the smallest $\frac{\Delta\omega_0}{J}$ ratio for all four complexes. However, we still could propose the nuclei C16 and C17 as suitable qubits, because even though the pair of nuclei C16–C17 exhibited a ratio smaller than 10 for complex 4, for example, the C16 and C17 nuclei are involved in other couplings, forming a contiguous network of couplings. In complex 4, the pair of nuclei C16–H39 presented a ratio of 4,337,957, and the pair of nuclei C17–H42 exhibited a ratio of 4,487,478, which fulfills the requirement outlined by Mawhinney and Schreckenbach [17].

3.4. Correlation Time and Spectral Density

The nuclear spin-1/2 systems can be precisely manipulated due to their coherence (lifetime of arbitrary superposition states). Despite this, they decohere slowly on the time scale of the spin interactions, the so-called relaxation time. Furthermore, NMR coherences vanish at the time of the spin–spin relaxation (T_2), so the NMR-QIP implementations are typically designed as pulse sequences shorter in time than T_2 [49].

Recently, the combination of NMR and MD investigations has been shown to provide a comprehensive description of the fast conformational dynamics of small molecules, as well as proteins and organic compounds [50]. However, MD simulations generate thousands of structures, and thus, to perform the subsequent quantum calculations, taking into account all of them is computationally expensive and infeasible, which makes the selection of the main conformations important. Thereby, in the present work, the selection of the main MD conformations was carried out by the statistical inefficiency (SI) method, which was previously developed and validated by the group of Coutinho and Canuto [51,52]. This method uses the statistical interval obtained from the energy autocorrelation; thus, it is possible to calculate the interval of the uncorrelated configurations, τ, by integrating $C(n)$ (Equation (5)) from zero to infinity. In light of this, the configurations that are separated by an interval of 2τ or more are pointed out as uncorrelated configurations.

$$C(n) = \sum_{i=1}^{N} C_i e^{-n/\tau_i},$$

(4)

$$\tau = \int_0^\infty C(t)dt.$$

(5)

The number of structures selected from the SI method are shown in Table 4. The Hg complexes presented the biggest number of conformations selected, 28 for complex 1 and 24 for complex 2. The molecule used in the validation of the theoretical methodology, TFE, exhibited 19 conformations selected. The smallest number of conformations selected was provided by Cd complexes, eight for both complex 3 and 4. In fact, the higher the correlation time, the smaller the number of selected structures was.

Table 4. Number of structures of the molecules selected by the SI method.

	Structures	Correlation Times (fs)
TFE	19	47.71
Complex 1	28	36.13
Complex 2	24	41.37
Complex 3	8	137.52
Complex 4	8	137.15

After selecting the structures, the next step is to obtain the relaxation times for the atoms of each structure. To obtain these parameters, we used another methodology called spectral density, which has already been successfully applied in other works [19,39]; therefore, the calculation of T_1 and T_2 (through the spectral density) is given by the following equations.

$$J(\omega) = \frac{2}{5}\left[\frac{S^2\tau_C}{1 + \tau_C^2 + \omega^2} + \frac{(1 - S^2)\tau}{1 + \tau^2\omega^2}\right] \tag{6}$$

In Equation (6), the rotational correlation time is given by τ_C, which is proportional to the inverse of the rotation diffusion constant, S^2 is the order parameter, and τ_e is the effective correlation time ($\tau^{-1} = \tau_C^{-1} + \tau_e^{-1}$)). From the spectral density, the relaxation rate R_1 and R_2 can be calculated by Equations (7) and (8).

$$R_1 = \frac{1}{T_1} = K[J(\omega_0) + J(2\omega_0)] \tag{7}$$

$$R_2 = \frac{1}{T_2} = \frac{K}{4}[J(0) + 10J(\omega_0) + J(2\omega_0)] \tag{8}$$

$$K = \left(\frac{\mu_0}{4\pi}\right)^2 \frac{3}{2} \frac{\hbar^2\gamma^4 I(I+1)}{\phi^6} \tag{9}$$

In the above equations, I is the spin quantum number, ω_0 is the Larmor angular frequency of the atoms, μ_0 is the vacuum permeability, $\hbar$ is the Planck constant, and ϕ is the average distance between the atoms of interest. The Larmor angular frequency refers to the precession rate of the proton magnetic moment around the external magnetic field (B_0) and the gyromagnetic radius of the atoms (γ), given by $\omega_0 = \gamma B_0$ [19]. The following topic shows the validation of the spectral density methodology, which is important, as it shows the agreement between the data obtained theoretically and the experimental results.

Validation of the Theoretical Methodology

The compound iodotrifluoroethylene (TFE) (Figure 2) was employed to validate the methodology used. In this step, the distances between the F1–F3 and F1–F2 atoms were taken into account to calculate the relaxation times values. Table 5 shows the theoretical and experimental results of the relaxation times for this molecule. The experimental values were taken from [53]. For F1–F3 atoms, the differences between theoretical and experimental values were: for T_1, 0.08 s, and for T_2, 0.05 s. For the F1–F2 atoms, the differences between theoretical and experimental values were 0.31 s for T_1 and 0.03 s for T_2. Consequently, the differences between the theoretical and experimental values were found to be very small, showing that the methodology used is effective in obtaining the relaxation parameters. Furthermore, the use of DFT offered an efficient way to determine the geometries; this conclusion is in agreement with [54–56], which used DFT to successfully calculate relaxation times and hyperfine coupling constants with a relatively low computational cost.

Table 5. Theoretical and experimental relaxation time values.

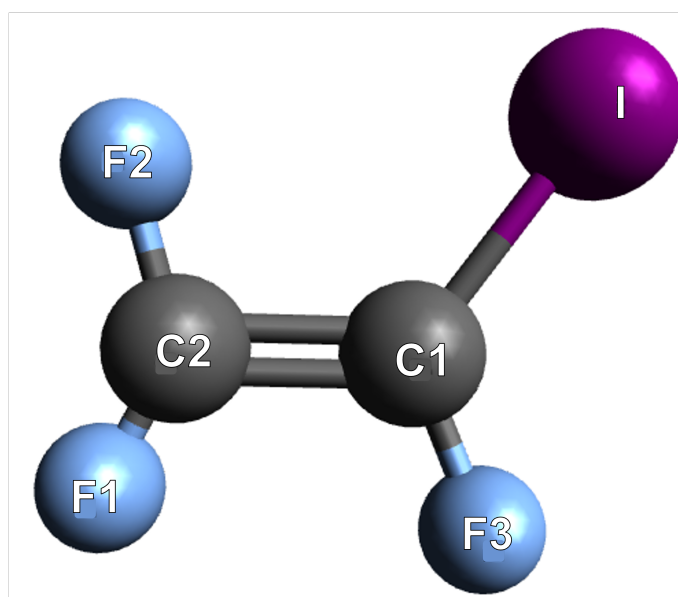|		T_1 (s)	T_2 (s)	R_1 (s^{-1})	R_2 (s^{-1})
TFE (F1–F3)	Theoretical	5.29	0.19	0.18	5.26
	Experimental [1]	5.37	0.14	0.19	7.14
TFE (F1–F2)	Theoretical	5.25	0.15	0.19	6.66
	Experimental [1]	5.56	0.12	0.18	8.33

[1] From [53].

Figure 2. Iodotrifluoroethylene (TFE) structure.

3.5. Spectroscopic Parameters: Relaxation Times

Qubit molecules composed of spin-1/2 nuclei are broadly accepted as one of the most powerful systems against environmental noise, which affords them with relatively longer coherence time and allows the accurate control of quantum gate operations [57]. The relaxation process occurs when an arbitrary ensemble evolves toward its equilibrium state. This process may lead the system to decoherence, destroying qubit superposition states [47]. In larger qubit systems, the relaxation rate for each added spin contributes to multiple quantum coherences of the system. However, on the other hand, these individual contributions could destroy qubit superposition states, leading the system to decoherence [58]. For single qubits such as nuclear spin states, a good measure of the lifetime of arbitrary superposition states is the 'longitudinal' (T_1) and 'transverse' (T_2) relaxation times [58].

The relaxation times (T_1 and T_2) values and, consequently, the R_1 and R_2 values ($R_1 = \frac{1}{T_1}$ and $R_2 = \frac{1}{T_2}$) for all nuclei of each complex were calculated (Table 6). Taking into account all the studied complexes, the Si nucleus presented the highest T_1 and T_2 values, 44.80 s for T_1 and 9.97 s for T_2, while the H the smallest, 0.95 s for T_1 and 0.35 s for T_2. Consequently, Si had the smallest R_1 and R_2 values, 0.02 s^{-1} for R_1 and 0.10 s^{-1} for R_2, while H the highest, 1.05 s^{-1} for R_1 and 2.85 s^{-1} for R_2. Analyzing the complexes individually, complex 1 provided the highest values of T_1 and T_2 for the Si nucleus, 44.8 and 3.52 s, respectively. For complex 2, the highest T_1 was 32.77 s for Hg and the highest T_2 was 9.34 s for Si. Concerning the Cd complexes, for complex 3, the nucleus with the highest T_1 was Si, 13.99 s and the highest T_2 was Te, 2.05 s. For complex 4, the highest T_1 was for Se, 21.56 s and the highest T_2 was for Si, 9.97 s.

As already mentioned, the longer the relaxation time of the atoms, the better the coherence phase of the system. In this sense, it is important to understand the relaxation time increasing in the systems. From Table 6, the Hg T_1 value is much higher for complex 2 when compared to complex 1, which can be explained based on the electronegativity of atoms directly bonded to Hg. In complex 1, the Hg atom is directly bonded to the Te atom, while in complex 2, the Hg atom is directly bonded to the Se atom. The Se atom is more electronegative than the Te atom, and this causes in complex 2 a higher electron density, which can contribute to the increase in the relaxation time values. The same reasoning can be applied to the other systems. For the complexes with Te, the Te relaxation times were longer for complex 3 than for complex 1, because the Te atom is directly bonded to Hg in complex 1, while Te is directly bonded to Cd in complex 3, and as the Cd atom is more electronegative than Hg, the electron density in complex 3 becomes greater than in complex 1.

As expected, the T_1 is longer than T_2. Therefore, for single qubits, the coherence phase time could be well measured by the transverse (or spin–spin state) relaxation time, which is the minimum lifetime of arbitrary superposition states [3]. In this way, the NMR relaxation timescale T_2 must be as long as possible in each nucleus of the qubit molecule, thus avoiding a high decoherence rate [59].

In light of this and considering that the time needed for basic quantum operations is of the order of 100 μs [60], the T_2 values presented by all the nuclei from the studied complexes are thus suitable to be used as qubits for NMR-QIP, which implies that the operational accuracy is in principle close to what is needed for a scalable fault-tolerant NMR quantum processor [60].

Thus, the effects of the modifications on the relaxation times are significantly important for NMR-QIP, as the longer relaxation time in each nucleus of the qubit molecule provides the system a relatively longer coherence time, allowing accurate control on the quantum gate operations in a large-scale NMR-QIP.

Table 6. Calculated relaxation times for the studied complexes.

	Hg	Cd	Te	Se	P	Si	F	C	H
Complex 1									
T_1 (s)	21.27	-	7.17	-	1.20	44.80	1.22	1.95	1.05
T_2 (s)	2.04	-	1.02	-	0.63	3.52	1.12	1.49	0.46
R_1 (s^{-1})	0.04	-	0.14	-	0.83	0.02	0.82	0.51	0.95
R_2 (s^{-1})	0.49	-	0.98	-	1.58	0.28	0.89	0.67	2.17
Complex 2									
T_1 (s)	32.77	-	-	30.44	2.77	11.87	2.12	2.58	1.30
T_2 (s)	1.51	-	-	2.59	1.28	9.34	1.60	1.27	0.45
R_1 (s^{-1})	0.03	-	-	0.03	0.36	0.08	0.47	0.38	0.76
R_2 (s^{-1})	0.66	-	-	0.39	0.78	0.11	0.63	0.78	2.22
Complex 3									
T_1 (s)	-	7.82	9.22	-	2.01	13.99	2.72	2.56	0.95
T_2 (s)	-	1.05	2.05	-	0.37	1.10	1.97	1.25	0.35
R_1 (s^{-1})	-	0.13	0.11	-	0.50	0.07	0.37	0.39	1.05
R_2 (s^{-1})	-	0.95	0.49	-	2.70	0.91	0.81	0.80	2.85
Complex 4									
T_1 (s)	-	6.06	-	21.56	2.70	15.89	1.67	2.53	1.20
T_2 (s)	-	2.09	-	1.83	0.58	9.97	1.08	1.24	0.38
R_1 (s^{-1})	-	0.17	-	0.05	0.37	0.06	0.59	0.36	0.83
R_2 (s^{-1})	-	0.48	-	0.55	1.72	0.10	0.93	0.81	2.63

4. Conclusions

All the specially designed complexes were found to be promising candidates as qubit molecules. Examining the required spectral properties for NMR-QIP, the suitable qubit molecules studied in this work presented appropriate NMR parameters for efficient NMR-QIP implementation. Following the requirements for NMR quantum computing and a first-order spectrum, the four studied complexes presented: (i) spin–spin coupling constants large enough, enabling two-qubit operations, which could preserve the coherence and reduce the time of quantum gate operations; (ii) an appropriate range of chemical shifts, where the frequency differences of the nuclei are ample, allowing the selective manipulation of the individual spins, the qubit addressability; (iii) nuclei relaxation times large enough to perform the logic quantum gates in a certain algorithm; as in NMR-QIP, the decoherence is a key problem the longer the relaxation time in each nucleus of the qubit molecule, providing the system a relatively longer coherence time and better information processing.

Hence, the structural modifications proposed for the complexes gathered appropriate NMR parameters for the NMR-QIP, which could overcome the restriction regarding the

number of suitable qubits for the forthcoming NMR quantum computers and what is needed for a scalable fault-tolerant NMR quantum processor.

References

1. Glaser, S.J.; Marx, R.; Reiss, T.; Schulte-Herbrüggen, T.; Khaneja, N.; Myers, J.M.; Fahmy, A.F. Increasing the Size of NMR Quantum Computers. In *Quantum Information Processing*; John Wiley & Sons, Ltd.: Weinheim, Germany, 2005; Chapter 5, pp. 58–69. [CrossRef]
2. Jones, J.A. Quantum computing with NMR. *Prog. NMR Spectrosc.* **2011**, *59*, 91–120. [CrossRef] [PubMed]
3. Vind, F.A.; Foerster, A.; Oliveira, I.S.; Sarthour, R.S.; Soares-Pinto, D.O.; Souza, A.M.; Roditi, I. Experimental realization of the Yang-Baxter Equation via NMR interferometry. *Sci. Rep.* **2016**, *6*, 20789. [CrossRef] [PubMed]
4. Lu, D.; Li, K.; Li, J.; Katiyar, H.; Park, A.J.; Feng, G.; Xin, T.; Li, H.; Long, G.; Brodutch, A.; et al. Enhancing quantum control by bootstrapping a quantum processor of 12 qubits. *npj Quantum Inf.* **2017**, *3*, 45. [CrossRef]
5. Peterson, J.P.; Sarthour, R.S.; Laflamme, R. Enhancing Quantum Control by Improving Shaped-Pulse Generation. *Phys. Rev. Appl.* **2020**, *13*, 054060. [CrossRef]
6. Sauer, S.P.A. *Molecular Electromagnetism: A Computational Chemistry Approach*; Oxford University Press: Oxford, UK, 2011.
7. Vaara, J. Theory and computation of nuclear magnetic resonance parameters. *Phys. Chem. Chem. Phys.* **2007**, *9*, 5399–5418. [CrossRef]
8. Helgaker, T.; Jaszuński, M.; Pecul, M. The quantum-chemical calculation of NMR indirect spin–spin coupling constants. *Prog. NMR Spectrosc.* **2008**, *53*, 249–268. [CrossRef]
9. Helgaker, T.; Coriani, S.; Jørgensen, P.; Kristensen, K.; Olsen, J.; Ruud, K. Recent Advances in Wave Function-Based Methods of Molecular-Property Calculations. *Chem. Rev.* **2012**, *112*, 543–631. [CrossRef]
10. Autschbach, J. Relativistic calculations of magnetic resonance parameters: Background and some recent developments. *Philos. Trans. R. Soc. A* **2014**, *372*, 20120489. [CrossRef]
11. Krivdin, L.B. Computational ^{1}H NMR: Part 1. Theoretical background. *Magn. Reson. Chem.* **2019**, *57*, 897–914. [CrossRef]
12. Krivdin, L.B. Recent advances in computational liquid–phase 77Se NMR. *Russ. Chem. Rev.* **2021**, *90*, 265–279. [CrossRef]
13. DiVincenzo, D.P. The Physical Implementation of Quantum Computation. *Fortschr. Phys.* **2000**, *48*, 771–783. [CrossRef]
14. Ladd, T.D.; Jelezko, F.; Laflamme, R.; Nakamura, Y.; Monroe, C.; O'Brien, J.L. Quantum computers. *Nature* **2010**, *464*, 45–53. [CrossRef]

15. Marx, R.; Pomplun, N.; Bermel, W.; Zeiger, H.; Engelke, F.; Fahmy, A.F.; Glaser, S.J. Engineering of an all-heteronuclear 5-qubit NMR quantum computer. *Magn. Reson. Chem.* **2015**, *53*, 442–447. [CrossRef]

16. Lino, J.B.d.R.; Rocha, E.P.; Ramalho, T.C. Value of NMR parameters and DFT calculations for quantum information processing utilizing phosphorus heterocycles. *J. Chem. Phys. A* **2017**, *121*, 4486–4495. [CrossRef]

17. Mawhinney, R.C.; Schreckenbach, G. NMR quantum computing: Applying theoretical methods to designing enhanced systems. *Magn. Reson. Chem.* **2004**, *42*, S88–S98. [CrossRef]

18. Lino, J.B.d.R.; Ramalho, T.C. Exploring Through-Space Spin–Spin Couplings for Quantum Information Processing: Facing the Challenge of Coherence Time and Control Quantum States. *J. Phys. Chem. A* **2019**, *123*, 1372–1379. [CrossRef]

19. Lino, J.B.d.R.; Gonçalves, M.A.; Ramalho, T.C. Value of NMR relaxation parameters of diamagnetic molecules for quantum information processing: Optimizing the coherent phase. *Theor. Chem. Acc.* **2021**, *140*, 1432–2234. [CrossRef]

20. Lino, J.B.d.R.; Sauer, S.P.A.; Ramalho, T.C. Enhancing NMR Quantum Computation by Exploring Heavy Metal Complexes as Multiqubit Systems: A Theoretical Investigation. *J. Phys. Chem. A* **2020**, *124*, 4946–4955. [CrossRef]

21. Cory, D.G.; Fahmy, A.F.; Havel, T.F. Ensemble quantum computing by NMR spectroscopy. *Proc. Natl. Acad. Sci. USA* **1997**, *94*, 1634–1639. [CrossRef]

22. Neese, F.; Wennmohs, F.; Becker, U.; Riplinger, C. The ORCA quantum chemistry program package. *J. Chem. Phys.* **2020**, *152*, 224108. [CrossRef]

23. Lenthe, E.V.; Baerends, E.J.; Snijders, J.G. Relativistic regular two–component Hamiltonians. *J. Chem. Phys.* **1993**, *99*, 4597–4610. [CrossRef]

24. Pantazis, D.A.; Chen, X.Y.; Landis, C.R.; Neese, F. All-Electron Scalar Relativistic Basis Sets for Third-Row Transition Metal Atoms. *J. Chem. Theory Comput.* **2008**, *4*, 908–919. [CrossRef]

25. Baerends, E.J.; Ziegler, T.; Atkins, A.J.; Autschbach, J.; Bashford, D.; Baseggio, O.; Bérces, A.; Bickelhaupt, F.M.; Bo, C.; Boerritger, P.M.; et al. *ADF2017, SCM, Theoretical Chemistry*; Vrije Universiteit: Amsterdam, The Netherlands, 2017. Available online: https://www.scm.com (accessed on 15 April 2022).

26. Van Lenthe, E.; Baerends, E.J. Optimized Slater-type basis sets for the elements 1–118. *J. Comp. Chem.* **2003**, *24*, 1142–1156. [CrossRef]

27. Bryce, D.L.; Autschbach, J. Relativistic hybrid density functional calculations of indirect nuclear spin–spin coupling tensors—Comparison with experiment for diatomic alkali metal halides. *Can. J. Chem.* **2009**, *87*, 927–941. [CrossRef]

28. Radula-Janik, K.; Kupka, T.; Ejsmont, K.; Daszkiewicz, Z.; Sauer, S.P.A. Molecular modeling and experimental studies on structure and NMR parameters of 9-benzyl-3,6-diiodo-9H-carbazole. *Struct. Chem.* **2015**, *26*, 997–1006. [CrossRef]

29. Morsing, T.J.; Reinholdt, A.; Sauer, S.P.A.; Bendix, J. Ligand Sphere Conversions in Terminal Carbide Complexes. *Organometallics* **2016**, *35*, 100–105. [CrossRef]

30. Radula-Janik, K.; Kupka, T.; Ejsmont, K.; Daszkiewicz, Z.; Sauer, S.P.A. DFT and experimental studies on structure and spectroscopic parameters of 3,6-diiodo-9-ethyl-9H-carbazole. *Struct. Chem.* **2016**, *27*, 199–207. [CrossRef]

31. Glent-Madsen, I.; Reinholdt, A.; Bendix, J.; Sauer, S.P.A. Importance of Relativistic Effects for Carbon as an NMR Reporter Nucleus in Carbide-Bridged [RuCPt] Complexes. *Organometallics* **2021**, *40*, 1443–1453. [CrossRef]

32. Rusakov, Y.Y.; Rusakova, I.L. Hierarchical basis sets for the calculation of nuclear magnetic resonance spin–spin coupling constants involving either selenium or tellurium nuclei. *J. Phys. Chem. A* **2019**, *123*, 6564–6571. [CrossRef]

33. Wodyński, A.; Repiskỳ, M.; Pecul, M. A comparison of two-component and four-component approaches for calculations of spin–spin coupling constants and NMR shielding constants of transition metal cyanides. *J. Chem. Phys.* **2012**, *137*, 014311. [CrossRef]

34. Repisky, M.; Komorovsky, S.; Kadek, M.; Konecny, L.; Ekström, U.; Malkin, E.; Kaupp, M.; Ruud, K.; Malkina, O.L.; Malkin, V.G. ReSpect: Relativistic spectroscopy DFT program package. *J. Chem. Phys.* **2020**, *152*, 184101. [CrossRef] [PubMed]

35. De Azevedo Santos, L.; van Der Lubbe, S.C.; Hamlin, T.A.; Ramalho, T.C.; Matthias Bickelhaupt, F. A Quantitative Molecular Orbital Perspective of the Chalcogen Bond. *ChemistryOpen* **2021**, *10*, 391–401. [CrossRef] [PubMed]

36. Cardin, A.D.; Ellis, P.D.; Odom, J.D.; Howard, J.W. Cadmium-113 Fourier transform nuclear magnetic resonance spectroscopy. *J. Am. Chem. Soc.* **1975**, *97*, 1672–1679. [CrossRef]

37. Pecul, M.; Urbańczyk, M.; Wodyński, A.; Jaszuński, M. DFT calculations of ^{31}P spin–spin coupling constants and chemical shift in dioxaphosphorinanes. *Magn. Reson. Chem.* **2011**, *49*, 399–404. [CrossRef] [PubMed]

38. Jameson, A.; Jameson, C.J. Gas-phase 13C chemical shifts in the zero-pressure limit: Refinements to the absolute shielding scale for 13C. *Chem. Phys. Lett.* **1987**, *134*, 461–466. [CrossRef]

39. Gonçalves, M.A.; Santos, L.S.; Peixoto, F.C.; Ramalho, T.C. NMR relaxation and relaxivity parameters of MRI probes revealed by optimal wavelet signal compression of molecular dynamics simulations. *Int. J. Quantum Chem.* **2019**, *119*, e25896. [CrossRef]

40. Grivet, J.P. NMR relaxation parameters of a Lennard-Jones fluid from molecular-dynamics simulations. *J. Chem. Phys.* **2005**, *123*, 034503. [CrossRef]

41. *MATLAB Optimization Toolbox*; The MathWorks: Natick, MA, USA, 2008. Available online: https://www.mathworks.com/products/optimization (accessed on 15 April 2022).

42. Mallek, R.; Sanhoury, M.; Dhia, M.B.; Khaddar, M. Cadmium(II) complexes with phosphine tellurides: Synthesis and multinuclear (^{31}P, ^{125}Te, and ^{113}Cd) NMR characterization in solution. *J. Coord. Chem.* **2014**, *67*, 1541–1549. [CrossRef]

43. Riedel, S.; Straka, M.; Kaupp, M. Can Weakly Coordinating Anions Stabilize Mercury in Its Oxidation State +IV? *Chem. Eur. J.* **2005**, *11*, 2743–2755. [CrossRef]

44. Vigo, L.; Salin, P.; Oilunkaniemi, R.; Laitinen, R.S. Formation and structural characterization of mercury complexes from Te(R)CH2SiMe3 (R=Ph, CH2SiMe3) and HgCl2. *J. Organomet. Chem.* **2009**, *694*, 3134–3141. [CrossRef]

45. O'Boyle, N.M.; Banck, M.; James, C.A.; Morley, C.; Vandermeersch, T.; Hutchison, G.R. Open Babel: An open chemical toolbox. *J. Cheminf.* **2011**, *3*, 33. [CrossRef]

46. Criger, B.; Park, D.; Baugh, J. Few–qubit magnetic resonance quantum information processors: Simulating chemistry and physics. In *Quantum Information and Computation for Chemistry*; John Wiley & Sons, Inc.: Hoboken, NJ, USA, 2014; pp. 193–227. [CrossRef]

47. Havel, T.F.; Cory, D.G.; Lloyd, S.; Boulant, N.; Fortunato, E.M.; Pravia, M.A.; Teklemariam, G.; Weinstein, Y.S.; Bhattacharyya, A.; Hou, J. Quantum information processing by nuclear magnetic resonance spectroscopy. *Am. J. Phys.* **2002**, *70*, 345–362. [CrossRef]

48. Nelson, J.H. (Ed.) *Nuclear Magnetic Resonance Spectroscopy*; Pearson Education: Upper Saddle River, NJ, USA, 2003.

49. Vandersypen, L.M.K.; Chuang, I.L. NMR techniques for quantum control and computation. *Rev. Mod. Phys.* **2005**, *76*, 1037–1069. [CrossRef]

50. Helgaker, T.; Jaszuński, M.; Ruud, K. Ab Initio Methods for the Calculation of NMR Shielding and Indirect Spin–Spin Coupling Constants. *Chem. Rev.* **1999**, *99*, 293–352. [CrossRef]

51. Coutinho, K.; Canuto, S.; Zerner, M.C. A Monte Carlo-quantum mechanics study of the solvatochromic shifts of the lowest transition of benzene. *J. Chem. Phys.* **2000**, *112*, 9874–9880. [CrossRef]

52. Coutinho, K.; Canuto, S. Solvent Effects from a Sequential Monte Carlo - Quantum Mechanical Approach. *Adv. Quantum Chem.* **1997**, *28*, 89–105. [CrossRef]

53. Devra, A.; Prabhu, P.; Singh, H.; Arvind.; Dorai, K. Efficient experimental design of high-fidelity three-qubit quantum gates via genetic programming. *Quantum Inf. Process.* **2018**, *17*, 67. [CrossRef]

54. Gonçalves, M.A.; da Cunha, E.F.; Peixoto, F.C.; Ramalho, T.C. Probing thermal and solvent effects on hyperfine interactions and spin relaxation rate of δ-FeOOH(100) and [MnH$_3$buea(OH)]$_2^-$: Toward new MRI probes. *Comput. Theor. Chem.* **2015**, *1069*, 96–104. [CrossRef]

55. Patinec, V.; Rolla, G.A.; Botta, M.; Tripier, R.; Esteban-Gómez, D.; Platas-Iglesias, C. Hyperfine Coupling Constants on Inner-Sphere Water Molecules of a Triazacyclononane-based Mn(II) Complex and Related Systems Relevant as MRI Contrast Agents. *Inorg. Chem.* **2013**, *52*, 11173–11184. [CrossRef]

56. Gonçalves, M.A.; Santos, L.S.; Prata, D.M.; Peixoto, F.C.; da Cunha, E.F.; Ramalho, T.C. Optimal wavelet signal compression as an efficient alternative to investigate molecular dynamics simulations: Application to thermal and solvent effects of MRI probes. *Theor. Chem. Acc.* **2017**, *136*, 1–13. [CrossRef]

57. Xin, T.; Wang, B.X.; Li, K.R.; Kong, X.Y.; Wei, S.J.; Wang, T.; Ruan, D.; Long, G.L. Nuclear magnetic resonance for quantum computing: Techniques and recent achievements. *Chin. Phys. B* **2018**, *27*, 020308. [CrossRef]

58. Nielsen, M.A.; Chuang, I.L. *Quantum Computation and Quantum Information*; Cambridge University Press: New York, NY, USA, 2010.

59. Negrevergne, C.; Mahesh, T.S.; Ryan, C.A.; Ditty, M.; Cyr-Racine, F.; Power, W.; Boulant, N.; Havel, T.; Cory, D.G.; Laflamme, R. Benchmarking Quantum Control Methods on a 12-Qubit System. *Phys. Rev. Lett.* **2006**, *96*, 170501. [CrossRef]

60. Cory, D.; Laflamme, R.; Knill, E.; Viola, L.; Havel, T.; Boulant, N.; Boutis, G.; Fortunato, E.; Lloyd, S.; Martinez, R.; et al. NMR Based Quantum Information Processing: Achievements and Prospects. *Fortschr. Phys.* **2000**, *48*, 875–907. [CrossRef]